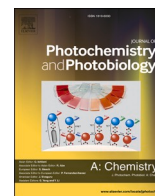




Contents lists available at ScienceDirect

## Journal of Photochemistry &amp; Photobiology, A: Chemistry

journal homepage: [www.elsevier.com/locate/jphotochem](http://www.elsevier.com/locate/jphotochem)

## Effect of solvent on the photophysical properties of isoxazole derivative of curcumin: A combined spectroscopic and theoretical study

Manisha Sharma<sup>a</sup>, Uttam Pal<sup>b</sup>, Mamta Kumari<sup>a</sup>, Damayanti Bagchi<sup>c</sup>, Swati Rani<sup>a</sup>,  
Dipanjana Mukherjee<sup>c</sup>, Arpan Bera<sup>c</sup>, Samir Kumar Pal<sup>c</sup>, Tanusree Saha Dasgupta<sup>d</sup>,  
Subho Mozumdar<sup>a,\*</sup>

<sup>a</sup> Department of Chemistry, University of Delhi, Delhi, 110007, India<sup>b</sup> Technical Research Centre, S. N. Bose National Centre for Basic Sciences, Block JD, Sector III, Salt Lake, Kolkata, West Bengal, 700106, India<sup>c</sup> Department of Chemical, Biological & Macromolecular Sciences, S. N. Bose National Centre for Basic Sciences, Block JD, Sector III, Salt Lake, Kolkata, West Bengal, 700106, India<sup>d</sup> Department of Condensed Matter Physics and Material Sciences, S. N. Bose National Centre for Basic Sciences, Block JD, Sector III, Salt Lake, Kolkata, West Bengal, 700106, India

## ARTICLE INFO

## Keywords:

Spectroscopy

Photophysics

TCSPC

DFT calculation

MD simulations

## ABSTRACT

The present work aims to decipher the photophysics of a  $\beta$ -diketo modified curcumin analog named isoxazole derivative of curcumin (IOC). IOC itself happens to be a potential drug molecule possessing numerous biological applications such as; anti-cancer, anti-malarial, anti-Alzheimer's, anti-Parkinson's etc. Herein, the photophysical properties of IOC have been explored in various sets of solvents. In order to investigate, steady state and time resolved spectroscopy have been utilized as a tool. To elucidate the experimental observations at molecular level, electronic structure calculations with density functional theory (DFT) as well as classical molecular dynamics (MD) simulations in explicit solvents have been deployed. The DFT has established that the most stable ground state electronic structure of the IOC molecule is the all *trans*- planar conformation where the conjugated pi-electrons are delocalized over the entire molecule. The MD simulations have provided an insight into the specific and non-specific interactions with the solvent molecules. Steady state spectroscopic techniques have shown that both the absorption and emission maxima experienced a traditional red shift upon increase in the solvent polarity. The absorption maxima for IOC got red shifted from 332 nm in hexane to 344 nm in DMSO. However, the red shift in the emission maxima is more pronounced than that of absorption maxima starting from 356 nm in hexane to 431 nm in water. The value of molar extinction coefficient has also been determined for IOC in different solvents from the concentration dependent absorption spectra. The time correlated single photon counting (TCSPC) data has revealed that the excited state of IOC molecule could relax via three probable pathways. Also, the overall process of decay of the excited state is comparatively slower in case of non-polar solvents. On the other hand, the fluorescence lifetime has been observed to be unusually low in case of dimethyl sulfoxide (DMSO) as compared to its other fellow polar aprotic solvents.

## 1. Introduction

The term solvatochromism is defined as the phenomenon where the position and intensity of electronic bands are dependent on the solvents [1,2]. During this process, the absorption and emission spectra, the steady state fluorescence intensity as well as the excited state lifetime of the fluorophore also get perturbed [3]. These photophysical properties of a fluorophore are governed by the intermolecular interaction of the

solute with its immediate environment [3]. The study of photophysical profile of fluorescent molecules in presence of different solvents helps in scrutinizing the phenomenon of solvatochromism. The solvatochromic fluorophores have been enormously investigated because of their capability to act as polarity-sensitive molecular probes [4]. The photophysical properties of various fluorophores have been reported to provide crucial contributions in the field of optoelectronic, analytical and biomedical sciences [5–7]. The idea of investigation of photophysics of

\* Corresponding author.

E-mail address: [subhomozumdar@yahoo.com](mailto:subhomozumdar@yahoo.com) (S. Mozumdar).<https://doi.org/10.1016/j.jphotochem.2021.113164>

Received 24 November 2020; Received in revised form 13 January 2021; Accepted 22 January 2021

Available online 26 January 2021

1010-6030/© 2021 Elsevier B.V. All rights reserved.

solvatochromic fluorophores which are biologically active have attracted immense attention from the scientific community. The information about the photophysical properties helps in monitoring the various biochemical processes and hence, reveals details about the mechanism of the drug activities of the molecules. The detailed insight about the solvatochromism of various biologically efficient molecules that have been reported include various coumarin derivatives like 7-aminocoumarin [8], coumarin-1 [9], coumarin-6 [10], coumarin-151 [11], along with others such as; sulphonated aluminium phthalocyanin [12], Chlorin e6 [13], merocyanin 540 [14], camptothecin [15], and many more. Based on the solvent dependent studies on the coumarin, derivatives, Karcz and Cravean et al. have done multiple investigation showing the photophysical and biological properties of widespread coumarin derivatives along with their metal complexes as well as thiazazole derivatives [16–19]. Besides all these molecules, the medicinal pigment which has been extensively investigated for the study of photophysical properties in presence of solvents of varying polarity is curcumin [20–22].

Curcumin is a polyphenolic compound found in the rhizome of *Curcuma longa Linn* exhibiting widespread biological applications like anti-cancer, anti-oxidant, anti-proliferative, anti-inflammatory etc. [23–25]. This phytochemical is also used in the treatment of skin cancer (through photodynamic therapy), cystic fibrosis, Parkinson's disease as well as Alzheimer's disease [26–28]. The extraordinary pharmacological activities of curcumin are attributed to its unique structure in which the  $\beta$ -diketo moiety is attached to the phenolic groups on its both sides through an  $\alpha,\beta$  unsaturated carbon chain [29]. A widespread photophysical studies have been done on curcumin so as to understand its biological efficiency. In general, curcumin displays strong absorption peaks in both UV and visible region. However, these absorption peaks are strongly influenced by the micropolarity of the environment of the curcumin molecules [30]. The absorption peak of curcumin has been reported to exhibits a solvent dependency by displaying a red shift in the absorption maxima in case of polar solvents. Khopde et al. have outlined that curcumin shows a red shift from 408 nm in cyclohexane to 430 nm in DMSO. Similar results were obtained for emission spectra where the emission maxima experiences a red shift from 446 nm in cyclohexane to 560 nm in methanol [20,21]. Moreover, it has also been reported that the curcumin molecule possesses low quantum yield as well as low excited state lifetime in the picosecond time scale. The fast decay of the fluorescence excited state has been attributed to the ultrafast Hydrogen atom transfer in the excited state (commonly known as ESIPT process) [31].

Despite all these beneficial advantages, curcumin could not be translated into a drug because upon oral administration (up to 8 g per day), the compound is poorly absorbed with only trace appearing in the blood [32]. The biological efficacy of curcumin has been limited by various factors such as poor aqueous solubility, lack of bioavailability and rapid degradation at physiochemical conditions [33,34]. The most pivotal factor responsible for its rapid degradation in aqueous medium has been assigned to the keto-enol tautomerization of the  $\beta$ -diketo moiety of the curcumin molecule [35]. Hence, in order to achieve maximum benefits of curcumin, extensive research has been carried out to design various diketo analogs of curcumin.

Numerous studies have reported that isoxazole derivatives of different drug molecules possess various biological applications including anti-bacterial, anti-fungal, anti-inflammatory, anti-convulsant, anti-viral and immunological activities [36]. Also, isoxazoles are inhibitors of p38 kinase, estrogen synthase, factor Xa enzyme, cytomegalovirus DNA polymerase and multidrug-resistance protein (MRP1) [36]. Because of all these applications immense research has been going on to discover new isoxazole derivatives which could be used as important pharmacophores in the modern drug discovery. Therefore, in order to cease the process of keto-enol tautomerization occurring in curcumin; the strategy to convert the diketo group of curcumin into an isoxazole ring has been utilized. This structural modification restricts

the rotational freedom of the molecule. It has been reported that the isoxazole derivative of curcumin (IOC) is known to have modest inhibitory activity against HIV-1 and HIV-2 proteases [37]. Chakraborty et al. have reported that as compared to curcumin, IOC has better in-vitro anti-proliferative activity [38]. Selvam et al. have reported that IOC exhibits significantly higher inhibitory activity towards the COX-2 enzyme as compared to curcumin [39]. IOC exhibits increased anti-tumor activity against hepatocellular carcinoma HA22T/VGH cell line [40]. It has also been evaluated for lipoxygenase inhibitory activity, cytotoxic activity, anti-tumor activity against breast cancer cell lines (MCF-7, SKBR3) and anti-malarial activity [41,42]. In a recent report, Shaikh et al. have extensively studied the *in-vitro* antioxidant and anti-radical activity of the IOC drug molecule. They have reported that these properties of IOC are even better than those of curcumin [43]. The preliminary studies on the interaction mechanism of IOC have been performed with various proteins such as; BSA [44], HSA [45,46],  $\beta$ -lactoglobulin [47] as well as with calf thymus DNA [48] but the detailed insight into the photophysics has not been done till date.

Now, in order to elucidate the fundamental understanding about the medicinal effects of the IOC drug molecule, its photochemistry and photophysics must be exploited. In order to serve this purpose, firstly the DFT calculations have been deployed to get an idea about the most stable ground state stereoisomer of the IOC molecule. Later, the interaction mechanism of IOC molecule with various solvents has been explored. The solute-solvent interaction can provide us with the information about the structural changes that occur in the molecule upon excitation in the presence of different microenvironments. The present study aims to study the process of solvatochromism for this potential drug molecule (IOC) in the presence of various solvents categorized into three different sets of solvents such as non-polar, polar protic and polar aprotic solvents. The steady state absorption and emission properties of this drug molecule have been investigated in wide range of solvents. The MD simulations have been performed on the IOC molecule in presence of six different solvents like water, methanol, DMSO, acetonitrile, benzene and hexane to get an idea about the type of interactions happening between the solute and solvent. The fluorescence transients of IOC in different solvents have also revealed the type of processes involved for the deactivation in their excited state. This has been done to acquire a microscopic understanding of the intermolecular effects of various physico-chemical parameters like solvent polarity, dielectric constant, hydrogen bonding ability etc. on the photophysics of IOC. Furthermore, to study the effect of hydrogen bonding on the solubility as well as photophysics of IOC along with the effect of deuteration has also been analyzed in depth.

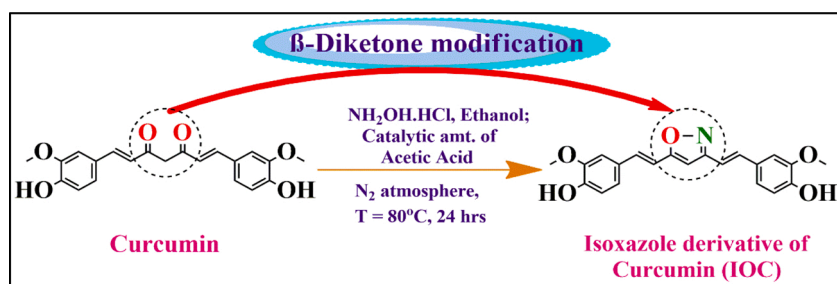
## 2. Experimental

### 2.1. Materials

Curcumin, Hydroxylamine Hydrochloride ( $\text{NH}_2\text{OH}\cdot\text{HCl}$ ) and Ethanol were purchased from Sigma Aldrich. All the solvents used were of analytical grade. All the chemicals were used as obtained without any further purification.

### 2.2. Synthesis of isoxazole derivative of curcumin

In a typical synthesis procedure, 1 mmol of curcumin was dissolved in 10 mL of ethanol and was allowed to stir for 15 min. To the resulting mixture, catalytic amount of acetic acid was added, followed by addition of 1.5 mmol of hydroxylamine hydrochloride ( $\text{NH}_2\text{OH}\cdot\text{HCl}$ ) [42]. The reaction mixture was allowed to stir at 80 °C for 24 h under  $\text{N}_2$  atmosphere (Scheme 1). The progress of the reaction was monitored by TLC. After the completion of the reaction, the reaction mixture was transferred to a beaker containing ice cold water. As a result, light yellow color precipitates were formed which were extracted via centrifugation. The crude obtained was recrystallized in methanol and hence, the pure



**Scheme 1.** Diagrammatic representation of  $\beta$ -diketone modification of curcumin into IOC along with schematic representation of the synthesis of IOC.

form of IOC was obtained. The prepared compound was characterized using  $^1\text{H}$  NMR,  $^{13}\text{C}$  NMR, and ESI-MS (SI: Note 1).

### 2.3. Preparation of solution of IOC in different solvents

In order to prepare the solutions of IOC in different solvents, firstly, a stock solution of IOC in methanol was prepared. Then, required amount of methanolic solution of IOC was poured in a vessel and the methanol was allowed to evaporate leaving behind a thin film of IOC. This thin film was scratched from the vessel and dissolved in appropriate amount of solvents. The solutions were ultrasonicated for about an hour to achieve maximum possible solubilization. Then after, the solutions were filtered through a  $0.45 \mu$  filter and were used for further characterizations. For the photophysical studies, the amount of IOC that was added to different solvents to prepare solutions was according to  $2 \mu\text{M}$  concentration. However, the concentration of IOC inside different solutions varied in accordance to its solvent dependent extent of solubility.

### 2.4. Characterization techniques

The absorption spectra were measured with Shimadzu spectrophotometer (UV-2600) in the range of 200–800 nm. All the spectra were recorded using 1 cm path length quartz cuvettes. The steady state emission spectra were recorded using Varian Carry Eclipse Fluorescence spectrophotometer at the absorption maxima of the respective samples in the range of 355–800 nm. During the measurements, both the excitation and emission slits were kept at 10 nm. The excitation spectra were obtained using Horiba fluorolog instrument at the emission maxima of

the corresponding samples.

The classification of solvents based on hydrogen bonding ability has been done in Table 1. This classification into the type of solvents has been referred from the literature [49].

The values of solvent polarity parameter ( $E_T(30)$ ) for each solvent has been taken from the literature [50]. The values of dimensionless normalized solvent polarity ( $E_T^N$ ) has been determined by using Eq. (1) which was proposed by Reichardt. In this equation, water and tetramethylsilane (TMS) are considered as extreme reference solvents with ( $E_T^N$ ) values of 1 and zero, respectively [51].

$$E_T^N = \frac{E_T(\text{solvent}) - E_T(\text{TMS})}{E_T(\text{water}) - E_T(\text{TMS})} = \frac{E_T(\text{solvent}) - 30.7}{32.4} \quad (1)$$

The reaction field parameter ( $\Delta f$ ) for different solvents has been calculated using the Lippert-Mataga equation described below [52].

$$\Delta f(\epsilon, n) = \frac{\epsilon - 1}{2\epsilon + 1} - \frac{n^2 - 1}{2n^2 + 1} \quad (2)$$

Where,  $\epsilon$  and  $n$  are the static dielectric constants and refractive index of the solvents; respectively. The values of  $\epsilon$  and  $n$  of pure solvents have been taken from the literature [13,53,54].

The fluorescence quantum yield of IOC in different solvents has been calculated using the equation written below [55].

$$\Phi_x = \Phi_s \left( \frac{A_x}{A_s} \right) \left( \frac{\text{Abs}_x}{\text{Abs}_s} \right) \left( \frac{\eta_x}{\eta_s} \right)^2 \quad (3)$$

In the above-mentioned equation, the symbols  $\Phi$ ,  $A$ ,  $\text{Abs}$ . and  $\eta$

**Table 1**

The values of characteristic properties of each solvent along with the steady state spectral properties of IOC.

Solvent	Type of solvent <sup>c</sup>	Dielectric constant ( $\epsilon$ )	Refractive Index ( $n$ )	Viscosity ( $\eta$ )	$E_T^N$	$\Delta f$	$\lambda_{\text{max}}$ (abs.) (nm)	$\lambda_{\text{max}}$ (emsn.) (nm)	$\epsilon$ ( $\text{M}^{-1} \text{cm}^{-1}$ ) ( $\times 10^4$ )	Stokes shift ( $\text{cm}^{-1}$ )
Acetonitrile	HBA-HBD <sup>d</sup>	38.8	1.34	0.37	0.466	0.30763	333	419	6.38	6164
Benzene	Ar-NHB-HBA <sup>e</sup>	2.28	1.501	0.65	0.111	0.00265	336	387	3.942	3922
<sup>a</sup> DCM	NHB <sup>c</sup>	9.08	1.424	0.45	0.3086	0.21842	334	403	4.229	5126
<sup>a</sup> DEE	HBA <sup>c</sup>	4.335	1.356	0.24	0.1173	0.16557	335	388	4.568	4078
<sup>a</sup> DMSO	HBA <sup>c</sup>	47.24	1.479	1.987	0.4444	0.26337	344	422	5.721	5373
<sup>a</sup> EG	HBA-D <sup>c</sup>	38.66	1.431	1.61	0.7901	0.27522	340	430	4.299	6156
Hexane	NHB <sup>c</sup>	1.88	1.37	0.31	0.0062	0.00041	332	356	2.298	2031
Methanol	HBA-D <sup>c</sup>	32.7	1.3284	0.547	0.7654	0.30859	337	429	4.521	6364
2-Propanol	HBA-D <sup>c</sup>	20.3	1.3776	2.3703	0.5525	0.27673	339	414	4.415	5344
<sup>a</sup> THF	HBA <sup>c</sup>	7.52	1.407	0.55	0.2068	0.20895	339	404	4.493	4746
Water	HBA-D <sup>c</sup>	80.7	1.33	0.89	1	0.32132	333	431	1.757	6828
<sup>b</sup> DMSO-d6	–	–	–	–	–	–	340	420	–	5602
<sup>b</sup> Methanol-d4	–	–	–	–	–	–	331	427	–	6792

<sup>a</sup> The abbreviations in the table corresponds to DCM = Dichloromethane, DEE = Diethyl ether, DMSO = Dimethyl sulfoxide, EG = Ethylene Glycol and THF = Tetrahydrofuran.

<sup>b</sup> DMSO-d6 = Deuterated DMSO and Methanol-d4 = Deuterated methanol.

<sup>c</sup> HBA = Hydrogen bond acceptor, HBD = Hydrogen bond donor, NHB = Non-hydrogen bonding, HBA-D = amphiprotic hydrogen bond acceptor and donor, Ar = Aromatic solvents.

<sup>d</sup> This solvent usually act as non-hydrogen bonding solvents, but has shown weak HBD properties with strong HBA indicator solutes.

<sup>e</sup> This aromatic solvent is usually weak hydrogen bond acceptors, but has also sometimes behaved as non-hydrogen-bonding solvents.

corresponds to fluorescence quantum yield, integrated area under the curve of fluorescence spectra, absorption intensity and refractive index; respectively. The subscript “x” has been designated for the unknown sample and “s” stands for standard. The standard used for these calculations is Quinine sulfate in 0.1 N H<sub>2</sub>SO<sub>4</sub> having quantum yield value of 0.546 [56].

For the picosecond resolved excited state lifetime measurements, the commercial time-correlated single-photon counting (TCSPC) set up from Edinburgh instruments with MCP-PMT detectors was used. Details of the time resolved fluorescence set up have been discussed in previous publications by Pal et al. [57]. For TCSPC measurements, the picosecond pulsed laser diode was employed as the excitation source of 375 nm with instrument response function (IRF) of 75 ps. The decay was obtained at emission wavelength of 500 nm at the polarizer angle of 55° while the excitation was vertically polarized. In order to eliminate all the possibility of the scattered excitation light, a long pass filter with cut-off at 400 nm was incorporated in the emission channel. The obtained picosecond resolved fluorescence transients were fitted using multi-exponential functions. The average lifetime of decay for IOC molecule has been determined using the equation described below [55].

$$\tau_{\text{avg.}} = a_1\tau_1 + a_2\tau_2 + a_3\tau_3 \quad (4)$$

The values of rate constant for radiative and non-radiative decay process have been determined using the two equations mentioned below [55].

$$k_r = \frac{\phi_F}{\tau_{\text{avg.}}} \text{ and } \frac{1}{\tau_{\text{avg.}}} = k_r + k_{nr} \quad (5)$$

Here,  $\tau_1$ ,  $\tau_2$  and  $\tau_3$  are the three components of the decay time of IOC in presence of different solvents and  $a_n$  represents their corresponding relative weightage. Here,  $k_r$  and  $k_{nr}$  are the radiative and non-radiative decay rate constants, respectively. The symbols  $\phi_F$  and  $\tau_{\text{avg}}$  corresponds to the fluorescence quantum yield and average lifetime of the excited state of IOC molecule.

All the measurements were done at 25 °C.

## 2.5. Computational studies

Structure of the stereoisomers of isoxazole derivative of curcumin (IOC) were geometry optimized at the level of density functional theory (DFT) using CAM-B3LYP exchange correlation functional and Pople's double zeta basis set 6-31+g(d) with diffuse and polarization function on heavy atoms [58]. CAM-B3LYP uses the long range corrected version of B3LYP with Coulomb-attenuating method (CAM-B3LYP) [59,60]. Apart from the gas phase (in vacuo) calculations, all the optimizations were done in polarizable continuum model (IEFPCM) of respective solvents, where the molecule was placed in a solvation cavity and a constant dielectric field was assumed on the outside [61,62]. In addition to water, DMSO and methanol explicit solvent molecules hydrogen bonded with IOC (three for water, two for DMSO and one for methanol) were also used besides the implicit solvent model. UV-vis spectra of the most stable conformation of IOC was computed using time dependent density functional theory (TD-DFT) on the ground state equilibrium geometries with same exchange correlations and basis sets, with which the geometry was optimized [63]. In TD-DFT, vertical excitation was calculated with linear response solvation followed by state specific solvation correction. For emission calculations, a TD-DFT geometry optimization with equilibrium linear response solvation was performed. The bandwidth used for the calculation of both absorption and emission spectra is 0.333 eV.

Classical MD simulations were performed using Desmond molecular dynamics [64] program as implemented in Schrodinger Maestro molecular modeling suit (Academic release 2018-1). The IOC molecule was placed in a periodic boundary box with 1 nm buffer region on each side so that the molecule does not interact with its periodic image. Bond

orders were assigned and force field specific partial charges were generated using the default preparation wizard and manually verified. For the simulation in different explicit solvents, the simulation box was filled with the respective pre-optimized solvent models (water, methanol, acetonitrile, DMSO, benzene and n-hexane). Pre-optimized solvent models for simple point charge (SPC) water, DMSO and methanol was available by default. Solvent models for acetonitrile, benzene and n-hexane were built by optimizing 512 solvent molecules each in cubic periodic boxes. All the solvated IOC systems were electroneutral and therefore no ions were required to balance the charge; no salt has been added either. The simulations were run in OPLS (optimized potential for liquid simulations) force field [65]. The systems were equilibrated following the default five step relaxation protocol starting with Brownian dynamics for 100 ps with restraints on solute heavy atoms at NVT (with T =10 K) followed by 12 ps dynamics with restraints at NVT (T =10 K) and then at NPT (T =1 K) using Berendsen method. Then the temperature was raised at 300 K for 12 ps followed by 24 ps relaxation step without restraints on the solute heavy metal [66]. The final MD simulations were run in NPT ensemble with constant pressure of 1 bar and temperature of 298.15 K for 1.2 ns each. RESPA (reference system propagator algorithm) integrator was used with near, far and out time steps of 2, 2 and 6 fs; respectively. The isotropic pressure was applied using the Martyna-Tobias-Klein barostat method with relaxation time of 2 ps. The Nose-Hoover chain thermostat method was used with relaxation time of 1 ps. Long-range coulombic interaction was treated with the PME (particle mesh Ewald) method. For short-range coulombic interactions, the cut off radius was 9 Å [64,67]. Interaction energies (van der Waals' and Coulombic), radial distribution function (RDF; g(r)) were computed on the simulation trajectories.

## 3. Results and discussion

The primary aim of the study was to get basic understanding about the stereochemistry of the ground state of the IOC molecule and then to explore the phenomena of solvatochromism on the IOC molecule. The extent and reasons of effect of solvent polarity on the photophysical properties of IOC has also been scrutinized with the help of various theoretical and experimental techniques.

### 3.1. DFT calculations

The first step in acquiring fundamental knowledge about a new molecule is to know about its ground state structure. In order to explore the ground state geometry of the IOC molecule, the DFT calculations have been used as a tool. These calculations revealed that the isoxazole derivative of curcumin (IOC) could probably exist in a planar conformation where the electrons could get delocalized over the entire molecule. Conceptually, in order to experience complete electron delocalization over the molecule, the isoxazole ring of the IOC molecule must be aromatic and for that the oxygen atom must donate its lone pair of electrons. This has been depicted in Fig. 1a and it can be mentioned that subsequent to electron donation, it is possible for the oxygen atom to acquire a partial positive charge and the nitrogen atom to get a partial negative charge. Further, in the ground state it is possible for the molecule to exist in the zwitter ionic form, with the overall molecule remaining electrically neutral in nature. This hypothesis has been very well augmented by the calculation of Mulliken charge densities (in vacuo) on each atom of the molecule through DFT calculations and is represented in Fig. 1b. Computed charge densities showed similar trend in implicit polar as well as non-polar solvents and the results have been tabulated in supplementary information (SI: Table S1).

Fig. 1b shows the ground state optimized geometry of the most stable stereoisomer of IOC. The ground state geometries of other possible isomers are shown in Supplementary Information (SI: Fig. S1). Relative energies and dipole moment of each isomer as calculated by the DFT have been tabulated in Table S2. The isomers from IOC 1 to IOC 4 show

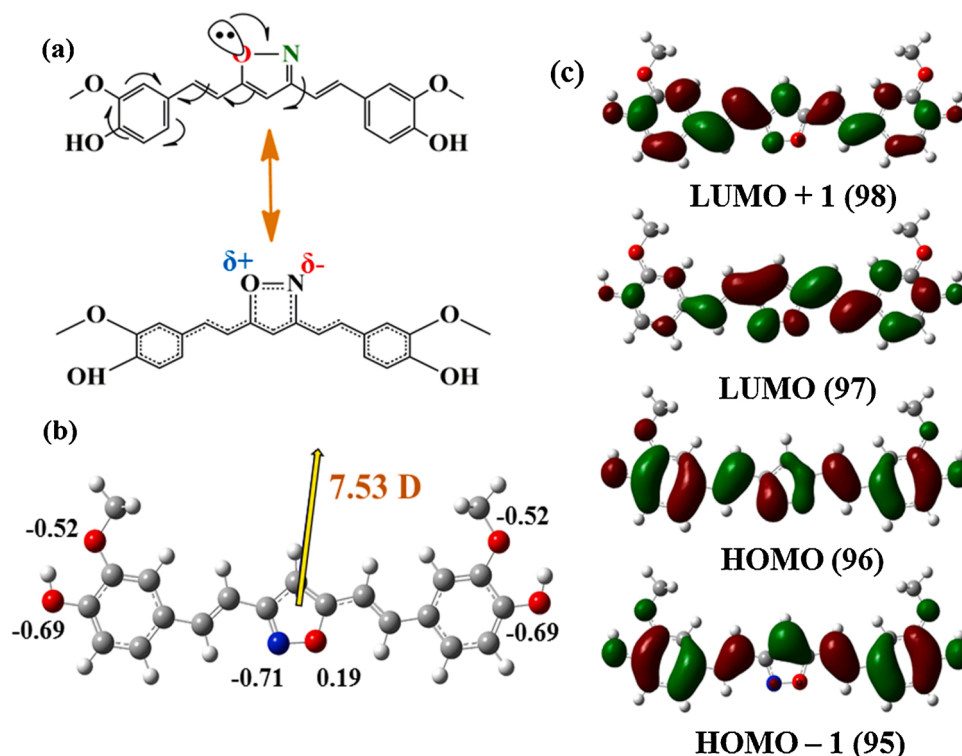


**Fig. 1.** Electronic structure of the most stable conformation of IOC. (a) Schematic representation of the electronic delocalization over the entire molecule of IOC and the appearance of partial positive charge on the O atom of the isoxazole moiety; (b) In vacuo ground state optimized geometry of IOC. Here, N is shown in blue and O in red. Computed partial charges on N and O are shown. Dipole moment vector is shown with the yellow arrow; and (c) Frontier molecular orbitals of IOC.

*trans*- geometries whereas the isomers from IOC 5 to IOC 8 show *cis*-geometries on either of the two double bonds present in the aliphatic chain of the IOC molecule. The isomer labelled as IOC 4 in which both the double bonds present in the aliphatic chain were having *trans*-geometries, was found to be energetically most favorable with a maximum dipole moment of 10.48 D. However, the conformers from IOC 1 to IOC 4

are interconvertible by the means of rotation along the single bonds. Amongst these conformers any conformation is possible but the most favorable one is the IOC 4. The thermal energy ( $k_B T$ ) at room temperature is 0.59 kcal/mol; therefore, the conversion of IOC 4 to any of the other three conformations (i.e. IOC 1 to IOC 3) would require extra amount of energy in terms of heat and light. Moreover, the stereoisomers

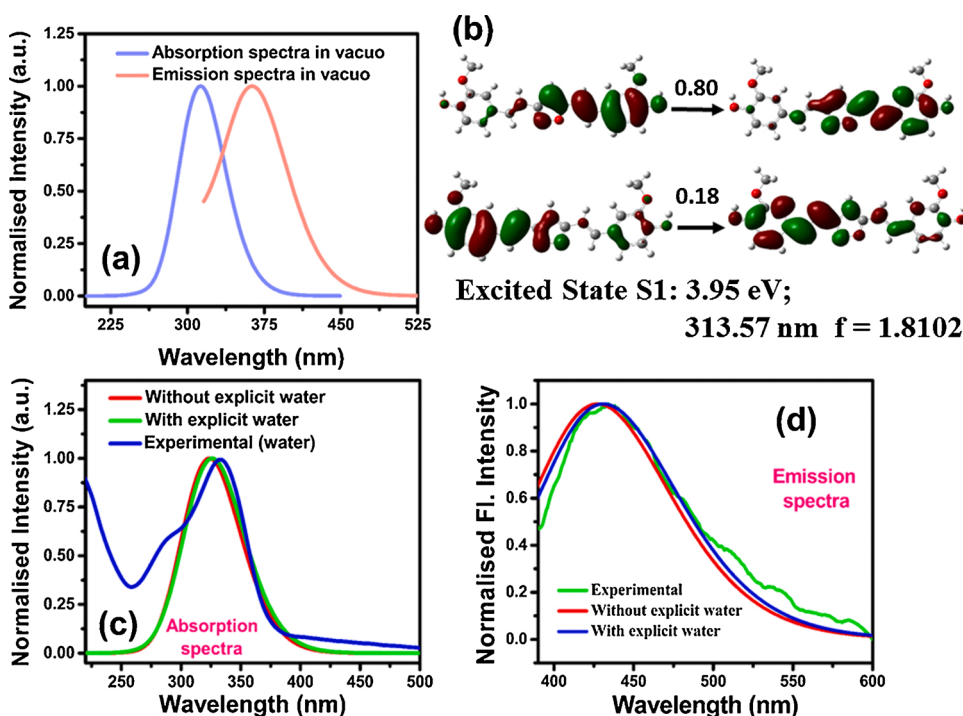


**Fig. 2.** Computed absorption and emission properties of IOC and the electronic transitions. (a) Computed absorption and emission spectra of IOC in gas phase (in vacuo); (b) Natural transition orbitals of IOC for the electronic transitions to the first transition state; (c) Comparison of computed absorption spectra of IOC in water with that of the experimentally observed spectrum and (d) Comparison of computed emission spectra of IOC in water with that of the experimentally observed spectrum.

from IOC 5 to IOC 8 are very unlikely as they are all *cis*- conformers and since curcumin exists as all *trans*- conformation; IOC being its derivative should also exist in *trans*-geometry. The relative energies of the conformers are represented in Table S2. Electron distributions in the frontier molecular orbitals (FMO) of IOC are depicted in Fig. 1c. It is evident from the figure that electrons in the highest occupied molecular orbital remains delocalized all over the IOC molecule.

Fig. 2a shows the computed absorption and emission spectra of the most stable conformer of IOC (i.e. IOC4) in gas phase (in vacuo). Absorption maxima in gas phase was observed at 314 nm and the emission maxima was at 365 nm. Large Stokes shift, therefore, may be attributed to the vibrational relaxation and change in the dipole moment (i.e. from 7.53 D to 7.73 D). Natural transitions orbitals (NTOs) for the  $S_0$  to  $S_1$  transition is depicted in Fig. 2b. NTOs show marked difference from that of FMOs. Partial delocalization of electron in NTOs over one side of the molecule indicates why the IOC shows much blue shifted absorption as compared to curcumin. Furthermore, in order to have a clear understanding, the experimentally obtained absorption and emission spectra of the synthesized IOC molecule in the presence of water has also been plotted with the computationally calculated absorption/ emission spectra (Fig. 2c and d). Fig. 2 clearly shows a very good agreement with each other reaffirming that the ground state of IOC is planar and it remains in all *trans*- conformation (*E,E*) with delocalization of the conjugated electrons across the isoxazole ring.

### 3.2. Steady state photophysical studies

Fig. 3 shows the UV-vis spectra of IOC in different solvents. It is clearly evident that the molecule could have an absorption maxima in the range of approximately 332 nm–344 nm (with a shoulder in the range of 275 nm–300 nm) depending on the solvent polarity. According to Maity et al., the peak at around 336 nm and the shoulder at around 295 nm (in the case of methanol as a solvent) can be ascribed to the  $\pi \rightarrow \pi^*$  and  $n \rightarrow \pi^*$  transitions, respectively [47]. The values of experimentally obtained absorption maxima of IOC in different solvents have been tabulated in Table 1. A large amount of red shift from 332 nm in hexane to about 344 nm in DMSO could be noticed for the  $\pi \rightarrow \pi^*$  transitions. These observations are in accordance with the fact that increment in the solvent polarity can result in a red shift in the peaks for the  $\pi \rightarrow \pi^*$  transition [68]. Also, based on the findings of the DFT calculations depicted in Fig. 2b, it is clearly evident that the peak at around 333 nm corresponds to the  $\pi \rightarrow \pi^*$  transition. The shift in the absorption maxima for DMSO has been found to be quite high in comparison to its fellow polar aprotic solvents like DCM, THF and acetonitrile. This suggests that there could be some specific interactions between DMSO and IOC, probably involving the phenolic or the isoxazole ring of the molecule. In addition, a large extent of hyperchromic shift could be observed in the absorption spectra in case of solvents like acetonitrile and diethyl ether. This could probably be attributed to the enhancement in the molar extinction coefficient in case of different solvents and should not be confused with the extent of solubility. Therefore, in order to get a clear understanding about the extent of solubility, values of molar extinction coefficient for IOC have been determined in all the aforementioned solvents. In doing so, the absorption spectra were recorded for the samples having varying concentration of IOC. Then after, a graph was plotted between absorbance and concentration of IOC. The overlay of the absorption spectra along with the linear plots have been provided in the supplementary information (SI: Note 2 and left-hand sides of Fig. S2 (non-polar solvents), S3 (polar aprotic solvents) and S4 (polar protic solvents)). These values have been tabulated in Table 1.

Fig. 4 shows the fluorescence emission spectra of IOC in different solvents. The effect of excitation wavelengths on the emission spectra was also monitored but no change in the nature of spectrum could be observed and the overlay of excitation wavelength dependent emission spectra has been depicted in supplementary information (Fig. S5). In general, the emission maxima for IOC increased with increase in the

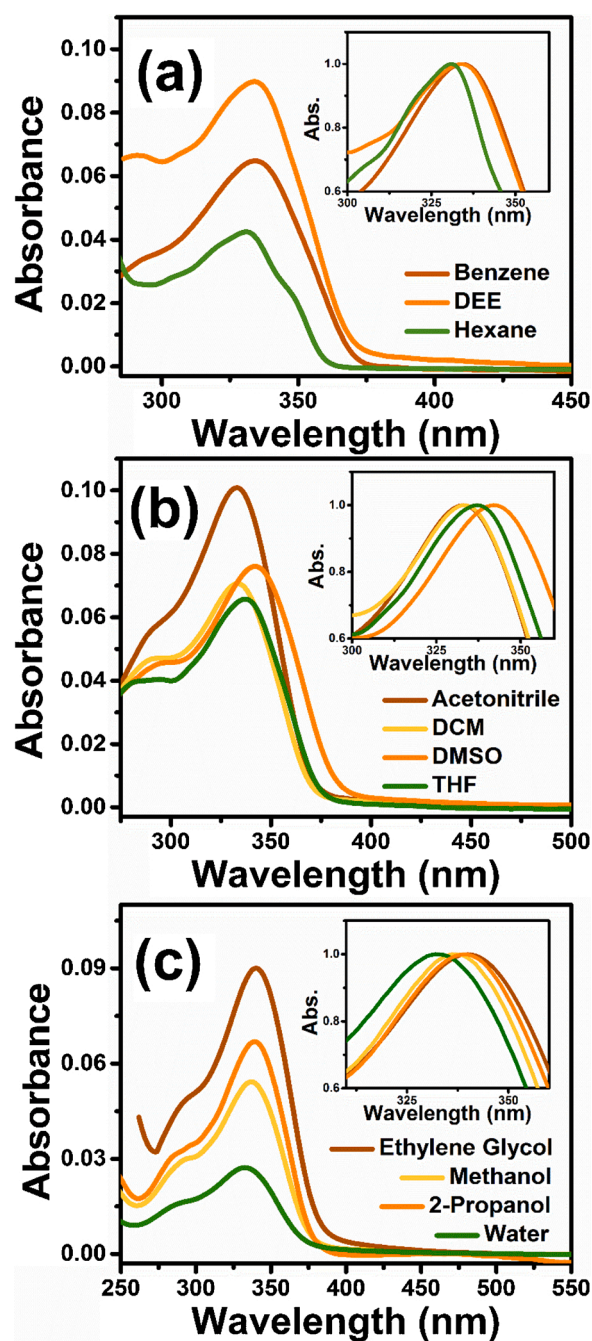


Fig. 3. The experimentally obtained absorption spectra of IOC in the presence of (a) non-polar solvents (Benzene, Diethyl ether and Hexane); (b) polar aprotic solvents (DCM, Acetonitrile, DMSO and THF) and (c) polar protic solvents (Ethylene glycol, Methanol, Water and 2-Propanol). Inset in each graph shows the corresponding intensity normalized graph of IOC in presence of respective solvents.

solvent polarity and the emission maxima varied in the range of 356 nm (in hexane) to 431 nm (in water). The values of emission maxima for each solvent are tabulated in Table 1. It is evident that, a large extent of red shift for the emission maxima could be observed in case of polar protic solvents (like ethylene glycol, methanol, 2-propanol and water). But an intermediate to a very low shift in the emission maxima could be observed for polar aprotic (like acetonitrile, DCM, DMSO and THF) and non-polar (like benzene, DEE and hexane) solvents, respectively. Interestingly, in case of polar aprotic and non-polar solvents a shoulder at the red end of the main peak (around 460 nm) could be observed in the

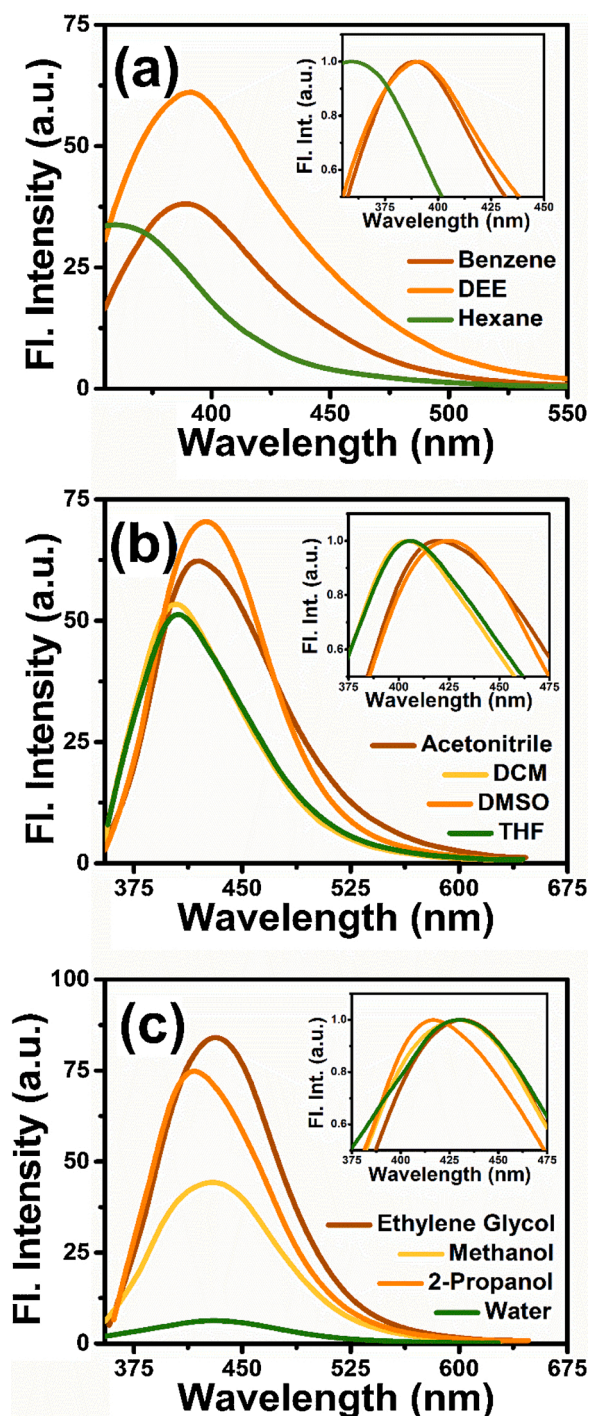


Fig. 4. The experimentally obtained emission spectra of IOC in the presence of (a) non-polar solvents (Benzene, Diethyl ether and Hexane); (b) polar aprotic solvents (DCM, Acetonitrile, DMSO and THF); and (c) polar protic solvents (Ethylene glycol, Methanol, Water and 2-Propanol). Inset in each graph shows the corresponding intensity normalized graph of IOC in presence of respective solvents. During the measurements, the samples were excited at their respective absorption maxima and both the emission and excitation slits were kept at 10 nm.

emission spectra. However, this shoulder was completely absent in the presence of polar protic solvents. Moreover, in order to check the effect of concentration of IOC in different solvents on its emission spectra, the concentration dependent emission measurements have been performed. The overlay of concentration dependent emission spectra in different solvents and their respective linear plots have been represented in

supplementary information. (SI: right hand sides of Fig. S2 (non-polar solvents), S3 (polar aprotic solvents) and S4 (polar protic solvents)). Similarly to the absorption spectra, a linear plot could be obtained for emission spectra as well, without any significant effect in the emission maxima or the nature of the emission spectra.

Furthermore, in order to completely overshadow the possibility of inner filter effect, the overlay of the normalized absorption and emission spectra of IOC in different solvents have been plotted. This overlay has been plotted in six different solvents which include benzene, diethyl ether, acetonitrile, DMSO, methanol and water. The plots have been represented in the supplementary information (SI: Fig. S6). This figure clearly demonstrates that the overlap in the absorption and emission spectra is very small. Also, the samples used for the analysis were very dilute (2  $\mu\text{M}$ ) having optical density  $\leq 0.1$ . Therefore, the chances of inner filter effect and reabsorption processes could be ruled out in these cases.

Based on the data obtained from the absorption and emission spectra, it could be seen that although changes in the polarity of solvents could lead to very little shifts in the absorption spectra, a large extent of red shift could be observed in the case of fluorescence spectra due to solvent relaxation. Computed absorption and emission spectra in presence of implicit solvents echo these findings. Computed ground state and excited state dipole moments of IOC in different solvents are listed in Supplementary Information (SI: Table S3). It shows very small change in the dipole moment of the excited state as compared to the ground state. However, marked decrease in the dipole moment is observed in case of n-hexane and benzene showing much less Stokes shift than in the polar solvents. This implies that the variation in the solvents is not affecting the ground state energy distribution significantly probably due to less polar nature of the ground state than the excited state [21,69]. Using the obtained values of absorption and emission maxima in the presence of different solvents, the values of Stokes shift have been calculated and are tabulated in Table 1 [17,19]. Similar studies have also been reported for curcumin where depending on the solvent polarity the Stokes' shift value have remarkably varied in the range of  $2000\text{ cm}^{-1}$  to  $6000\text{ cm}^{-1}$ . In case of curcumin, the values of Stokes shift have been reported to be comparatively larger for H-bond donating-accepting solvents like alcohols, DMSO etc [70]. The values of Stokes shift somewhat follows similar trend as that of curcumin. The huge variation in the values of Stokes shift suggest that the dipole moment of the excited state of the molecule could be higher than that of the ground state. This assumption is found to be well augmented by the computed values (SI: Table S3). Plotting the experimental values of Stokes shift against the  $E_T^N$  values for different solvents, a linear correlation could be observed with the regression coefficient value of 0.75 (Fig. 5a). In order to verify whether this Stokes shift was because of the solvent polarity (and not due to other factors like dielectric constant/ viscosity) the values of Stokes shift for different solvents were plotted against the reaction field parameter ( $\Delta f$ ) in accordance with the Lippert-Mataga equation. A linear increase in the Stokes shift with the reaction field parameter with the regression coefficient of 0.96 ( $n = 10$ ) could be observed (Fig. 5b). Deviation from linearity in this case could be observed in case of aromatic solvents i.e. benzene. This could probably be because of the hydrophobic ( $\pi$ -stacking) interactions between the phenyl rings of solvent and that of the IOC molecule.

In order to get information about the emitting species in the excited state, the excitation spectra were recorded. The excitation spectra of IOC in different solvents have been provided in the supplementary information (SI: Fig. S7). The effect of emission wavelength on the excitation spectra was also monitored in both the red as well as blue wavelength ends but no significant change in the nature of spectrum could be observed. The overlay of the excitation spectra at different emission wavelength has been specified in the supplementary information (SI: Fig. S8). However, the width of the excitation spectra was larger as compared to the absorption spectra. Similar to the absorption spectra,

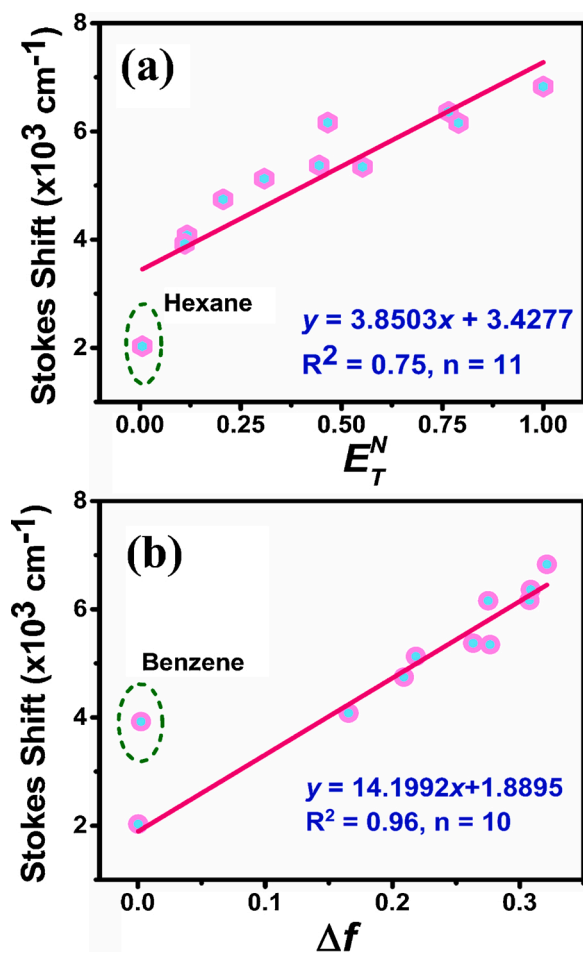


Fig. 5. (a) Plot of Stokes shift ( $\text{cm}^{-1}$ ) vs.  $E_T^N$  values for different solvents and (b) represents the plot of Stokes shift ( $\text{cm}^{-1}$ ) vs.  $\Delta f$  (reaction field parameter) according to the Lippert-Mataga equation.

two peaks in the excitation spectra could be observed, one at around 340 nm and the other one around 290 nm. Therefore, from the absorption, emission and excitation spectra, it could be concluded that there was only one specie in the sample and there was no contamination from any other absorbing or emitting species.

### 3.3. MD calculations

The classical MD simulations with explicit solvents have been used to determine the coulombic as well as van der Waals' interaction energies with the solvents. Fig. 6 depicts the graphs showing the interaction energies of IOC in the presence of different solvents. As clearly shown in Fig. 6a, both the energies could equally contribute in case of water. In case of other polar protic solvents like methanol (Fig. 6b), the van der Waals' forces have slightly more contribution in the interaction with the IOC molecule which could probably be due to the presence of additional methyl group in methanol. In case of polar aprotic solvents like DMSO and acetonitrile (Fig. 6c & d), the major contribution for interactions between IOC and solvent molecules was found to be from the van der Waals' one. Whereas, in case of non-polar solvents like benzene and hexane (Fig. 6e & f), since, these solvents cannot have any type of participation from the coulombic energy, only van der Waals' forces were found to be responsible for the interactions between IOC and solvent molecules. With the reducing polarity of the solvent, coulombic contributions decrease and van der Waals' interactions increase. These observations are in synchrony with the expected behavior of a molecule in solvents with the decreasing polarity.

In order to get information about the probability to find a particle at a certain distance from the particle used as reference, radial distribution function (RDF) could be utilized [71]. In MD simulations, the atom-atom RDF could be used to study the distances between two atoms which give an atomic level insight into the stable non-bonded interactions [72]. The solute-solvent radial distribution function;  $g(r)$  (RDF) graphs were obtained from MD simulations. Fig. 7 represents the RDFs for IOC in the presence of various solvents. The RDFs for IOC in presence of water is represented in Fig. 7a. A peak  $\sim 2$  Å is clearly visible in this graph which could correspond to the hydrogen bond distance of N atom and —OH group of the IOC molecule with the water molecules. This could be attributed to the H-bonding between these functional groups and the water molecules. A small peak at this same position is also observed for the methoxy (—OMe) group of the IOC. This may probably be due to the close proximity of the methoxy group with the hydroxyl group of the IOC molecule that forms a hydrogen bond. A similar kind of RDFs is also obtained in case of methanol (Fig. 7b). In this case, the peak could be observed to shift from  $\sim 2$  Å to  $\sim 3$  Å which typically corresponds to the hydrogen bond donor-acceptor distance. In case of polar aprotic solvents like DMSO and acetonitrile (Fig. 7c & d) the observations are completely different. The MD simulations have divulged that DMSO being a hydrogen bond acceptor type of molecule, could form hydrogen bond with the peripheral hydroxyl group of the IOC molecule. This is evident from the RDFs in case of DMSO, where there is a peak  $\sim 2.5$  Å only for the —OH group and not for the nitrogen atom. It could be because of these interactions that DMSO shows such a high red shift in the absorption as well as emission spectra despite being a polar aprotic solvent. As apparent from the RDFs in the presence of acetonitrile, there are no specific strong interactions with the IOC molecule. Furthermore, the observations in case of benzene are quite surprising (Fig. 7e). The RDFs shows the formation of somewhat ordered structure of the benzene solvent molecules surrounding the IOC molecule from the center of mass of the benzene molecule, the peak is at  $\sim 5$  Å. This could be attributed to the  $\pi$ - $\pi$  stacking of the benzene ring with the phenolic as well as isoxazole ring of the IOC molecule. All these observations could also be observed in the MD simulation snapshots taken at definite time intervals (SI: Video S1-S6). In case of aliphatic non-polar solvent like hexane also, the solvent molecules are equidistant from all the atoms/groups of the IOC molecule but the formation of an ordered structure is missing. Therefore, these interactions could only correspond to the weak hydrophobic type.

Meanwhile, to complement these results, the H-bond distance calculations with solvents were done using the DFT method. The bond distance between the nitrogen atom and the —OH group of the water and methanol molecule was found to be 1.83 Å and 1.80 Å; respectively. Whereas in case of DMSO, the bond distance between the —OH group of IOC molecule and the oxygen atom of the DMSO molecule was found to be 1.77 Å. Therefore, it could be said that the DFT results of bond distance calculations convey that the strength of H-bond formed by DMSO is much stronger than that formed by other polar protic solvents like water and methanol.

### 3.4. Fluorescence quantum yield and time-resolved studies

The fluorescence quantum yield of IOC in presence of all the aforementioned solvents with varying solvent polarity have been calculated using quinine sulfate in 0.1 N  $\text{H}_2\text{SO}_4$  as the reference. The values obtained have been tabulated in Table 2. From the values it could be observed that the fluorescence quantum yield is lower in non-polar solvents rather than in polar solvents (including both polar protic and polar aprotic solvents). Also, the values are even higher in polar protic solvents (excluding water) like in ethylene glycol, methanol and propanol. The exceptionally high value has been obtained in case of DMSO indicating the presence of some specific solute-solvent interactions between DMSO and IOC molecules. Overall, it could be said that IOC has comparatively higher fluorescence yield in the solvents that falls under

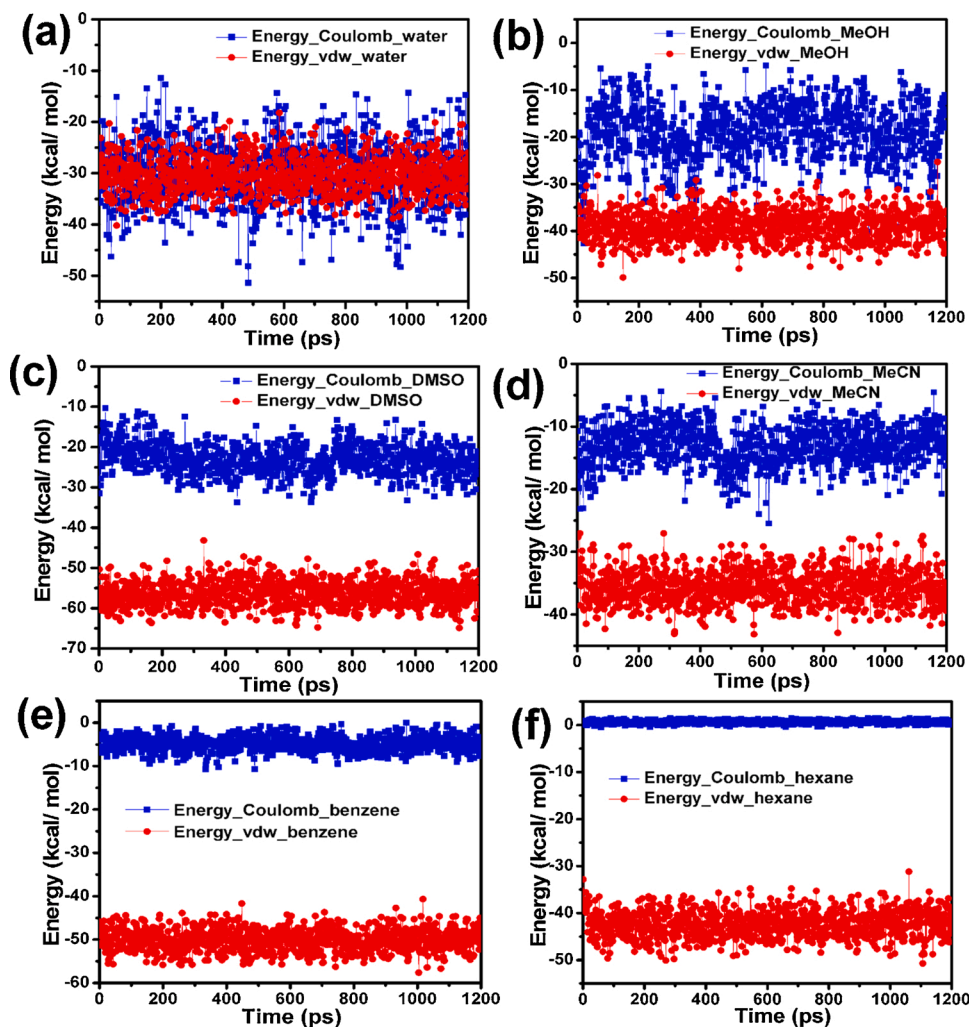


Fig. 6. The computed coulombic and van der Waals' interaction energies of IOC in the presence of (a) water; (b) Methanol; (c) DMSO; (d) Acetonitrile; (e) Benzene and (f) Hexane as obtained through MD stimulations.

the category of Hydrogen bond accepting-donating type.

Moreover, in order to get an insight about the excited state dynamics of the IOC molecule, the picosecond resolved fluorescence decay transients of IOC molecule under different solvents were recorded (Fig. 8). Time resolved fluorescence decay of IOC could be characterized by triexponential fitting parameters. Such kind of transients of IOC in homogenous solvent have also been observed for some other fluorescent dyes including some coumarin derivatives [73,74]. This implies that three different kinds of processes are involved in the deactivation of the excited state of this potential drug molecule. The values of each component of the decay profile of IOC molecule along with their percentage contribution in different solvents are tabulated in Table 2. While working with different solvents it could be noted that the first component was around 30 ps, the second component ranged from 150 ps-700 ps and the range of the third component was from 1 ns to 3 ns. Further, while contribution from the third component was almost negligible for the polar protic and polar aprotic solvents, pronounced contribution could be articulated by the category of non-polar solvents (especially hexane). In general, the average lifetime for the decay of the excited state of IOC molecule was observed to be maximum for non-polar solvents. Fig. 8a delineates the excited state decay profiles of IOC in non-polar solvents like benzene, diethyl ether and hexane. The slowest decay could be observed in case of benzene for which the average fluorescence lifetime was close to 826 ps. On the other hand, while dealing with polar solvents, the polar aprotic solvents like DCM,

THF, acetonitrile etc. (Fig. 8b) gave larger values of average lifetime in comparison to the polar protic solvents like methanol, ethylene glycol, water etc. This could be ascribed to the deactivation of the excited state majorly through non-radiative processes in polar solvents [75]. In other words, it could be said that in the case of polar solvents, the excited state of the IOC molecule majorly deactivates through non-radiative pathway thereby decreasing the average excited state lifetime. Whereas, in case of non-polar solvents the radiative processes predominate for the deactivation of the excited state of IOC and therefore, comparatively higher values of average lifetime could be obtained [76]. It has been reported that in such cases it is assumed that the nature of excited state of IOC is different in non-polar solvents than in other solvents [9]. Typically, the trend for the value of average excited state lifetime in polar protic solvents followed the order as Ethylene Glycol > Methanol > Propanol > Water. Based on this information it could be interpreted that the fast decay in case of polar protic solvents could probably be due to the hydrogen bonding between IOC molecule and the solvent molecules. Moreover, the fastest lifetime could be obtained in case of DMSO and this could be attributed to the formation of a stronger H-bond between DMSO and the hydroxyl group of the IOC molecule. Based on the fluorescence quantum yield and lifetime measurements, the values of rate constant for the decay of the excited state through radiative ( $k_r$ ) and non-radiative ( $k_{nr}$ ) pathways have been calculated. These values have been tabulated in Table 2. It could be observed that the values of both  $k_r$  and  $k_{nr}$  strongly depend on the type of solvent used.

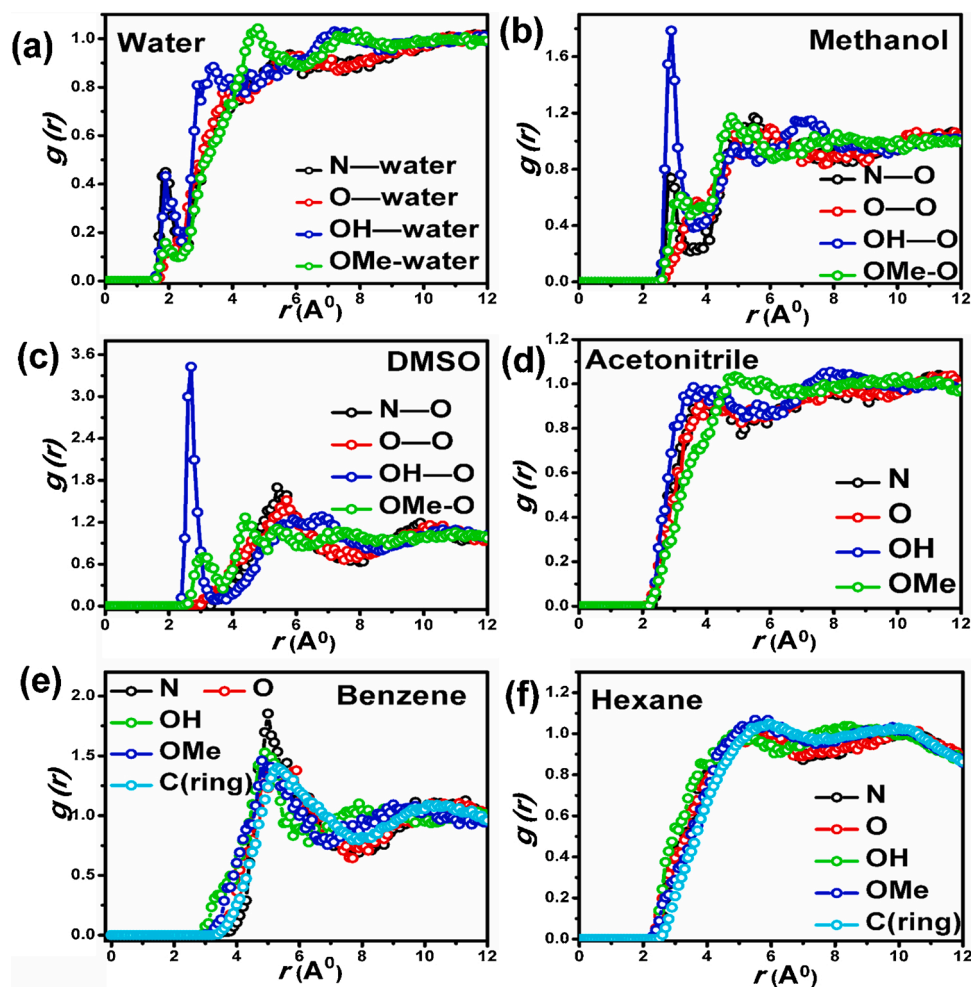


Fig. 7. The computed RDF plots of particular atom/ group of the IOC molecule in the presence of (a) water; (b) Methanol; (c) DMSO; (d) Acetonitrile; (e) Benzene and (f) Hexane as obtained through MD stimulations.

Table 2

Lifetime of picosecond time-resolved fluorescence transients of IOC in the presence of different solvents.

Sample name	$\tau_1$ (ps)	$\tau_2$ (ps)	$\tau_3$ (ps)	$\tau_{avg.}$ (ps)	$\chi^2$	$\phi_x$	$k_r$ ( $s^{-1}$ ) ( $\times 10^9$ )	$k_{nr}$ ( $s^{-1}$ ) ( $\times 10^9$ )
Acetonitrile	30 (78.23)	305.5 (15.64)	1532 (6.12)	165.07	1.077	0.046	2.82	5.78
Benzene	40 (30.77)	705.5 (26.92)	1476.6 (42.31)	826.96	1.05	0.04	0.49	1.16
<sup>a</sup> DCM	33.5 (65.14)	361.2 (18.55)	1461.2 (16.31)	327.15	1.098	0.056	1.70	2.89
<sup>a</sup> DEE	36.7 (56.31)	350.3 (17.47)	1415.4 (26.21)	452.9	1.019	0.042	0.93	2.11
<sup>a</sup> DMSO	30 (81.21)	142.4 (18.18)	1524.1 (0.61)	59.49	1.277	0.076	12.56	15.52
<sup>a</sup> EG	33 (40.56)	178.6 (57.55)	1277.2 (1.89)	140.25	1.175	0.075	5.38	6.61
Hexane	37 (60.91)	333.5 (20)	3092.1 (19.09)	679.5	1.046	0.032	0.47	1.42
Methanol	32 (71.94)	149.7 (23.74)	1099.9 (4.31)	106.03	1.113	0.06	5.68	8.86
2-Propanol	35.5 (72.26)	197.2 (26.27)	1509.1 (1.46)	99.51	1.234	0.075	7.58	9.29
<sup>a</sup> THF	32 (81.75)	257 (12.84)	1762.8 (5.41)	154.45	1.137	0.057	3.72	6.10
Water	30 (92.61)	205.5 (6.25)	1964.7 (1.14)	62.95	1.282	0.004	0.68	15.84
<sup>b</sup> DMSO- <i>d</i> 6	30 (78.65)	144.7 (20.12)	1425 (1.22)	70.1	1.216	–	–	–
<sup>b</sup> Methanol- <i>d</i> 4	32.5 (70.92)	172.8 (27.66)	1731.3 (1.42)	95.4	1.122	–	–	–

<sup>a</sup> The abbreviations in the table corresponds to DCM = Dichloromethane, DEE = Diethyl ether, DMSO = Dimethyl sulfoxide, EG = Ethylene Glycol and THF = Tetrahydrofuran.

<sup>b</sup> DMSO-*d*6 = Deuterated DMSO and Methanol-*d*4 = Deuterated methanol.  $\phi_x$  corresponds to quantum yield of IOC in presence of different solvents.

The values also indicate that the non-radiative processes predominated over the radiative ones in case of polar protic solvents and therefore, the lifetime is lower in those solvents.

### 3.5. Effect of deuterated solvents

In order to gain further insight about the nature of interaction

between the IOC molecules and the various solvent molecules, the effect of deuteration was studied in detail. With this intention, two deuterated solvents (DMSO-*d*6 and Methanol-*d*4) were chosen on the grounds of one being from the hydrogen bond acceptor family and another from the hydrogen bond donor family of solvents. For this analysis, different steady state and time-dependent spectroscopic techniques were utilized. Firstly, the steady state absorption spectra of the IOC molecules in the

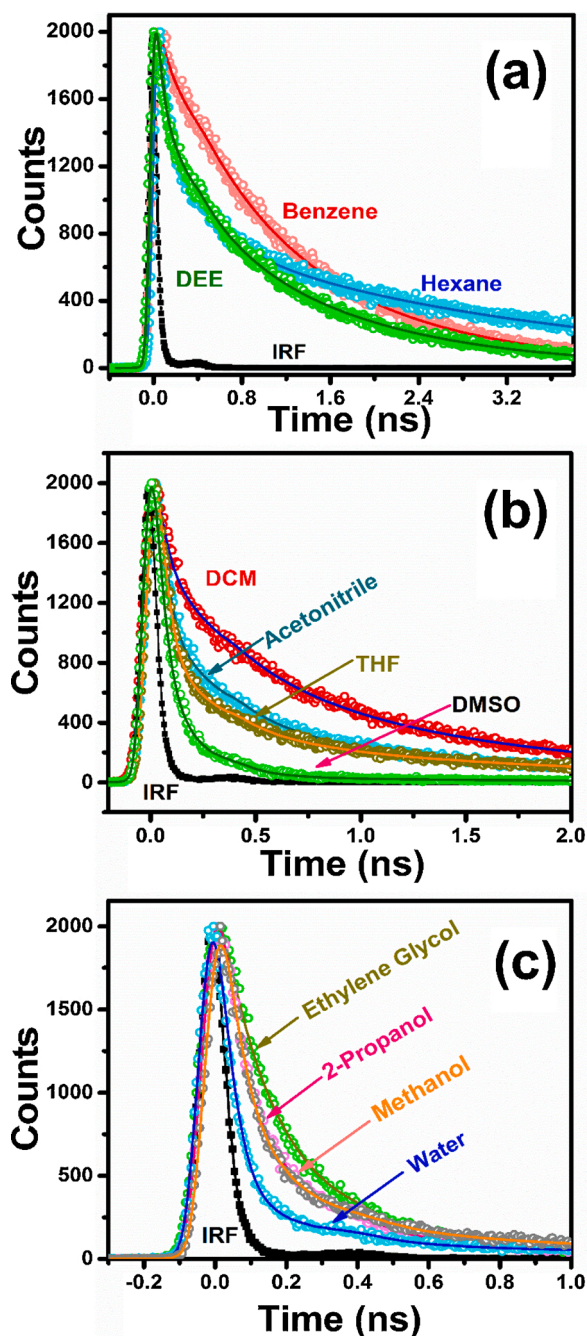


**Fig. 8.** TCSPC studies performed on the IOC molecule in presence of (a) non-polar solvents (Benzene, Diethyl ether and Hexane); (b) polar aprotic solvents (DCM, Acetonitrile, DMSO and THF) and (c) polar protic solvents (Ethylene glycol, Methanol, 2-Propanol and Water). The fluorescence decay transients have been obtained at the emission wavelength of 500 nm using a filter of 400 nm.

deuterated solvents were recorded. Though the variation in the  $\lambda_{\max}$  of the IOC molecules was insignificant as compared to their non-deuterated counterparts, there was a drastic blue shift in the shoulder (SI: Fig. S9a & b) together with a profound decrease in the absorption intensity. The decrease in the intensity of absorption could be ascribed to the low solubility of IOC molecules in the deuterated solvents. This information helps us in inferring that the solubility of the IOC molecule in different solvents depends not only on the polarity but also on the H-bonding ability of the solvent. Further, in the deuterated solvents, a drastic decrease in the fluorescence intensity could be observed without any

major change in the position of fluorescence maxima (SI: Fig. S9c & d). This could confirm that intermolecular hydrogen transfer is not the sole reason for the red shift in the emission maxima for other polar solvents. Also, it could be said that the solubility of IOC molecule does depend on the H-bonding ability of the solvent molecules. Based on the absorption and emission spectra it could be interpreted that deuteration of the solvents could only affect the ground state of the molecule but not the excited state. Further, upon deuteration, the nature of excitation spectra was found to be almost similar to that in the non-deuterated solvents (SI: Fig. S9e & f).

Fig. S9g (Supplementary Information) shows overlay of the decay transients of the excited state of IOC molecule upon deuteration. It has already been established that typically the average lifetime of curcumin is extremely fast because of the ESIPT (Excited State Intramolecular Proton Transfer) process [21]. The main contribution of ESIPT is from the diketo group of this molecule. Therefore, upon deuteration, the decay of the excited state of curcumin is seen to get slower [20]. Since in the case of IOC molecule, the diketo group of curcumin is blocked by the formation of 5-membered isoxazole ring, there should not be any ESIPT process. This observation could be verified by the TCSPC studies performed on the IOC molecule in presence of non-deuterated as well as deuterated solvents. The average lifetime of the IOC molecule in the presence of DMSO and DMSO-*d*6 as well as in methanol and methanol-*d*4 were found to be almost equivalent. This could be explained by the fact that DMSO, being an H-bond acceptor type of solvent, could only form H-bonds with the peripheral —OH groups of IOC molecule leaving the lifetime of the IOC molecule in presence of DMSO-*d*6 unaltered. Upon deuteration, the nature and the extent of H-bonding would not be permuted. However, in case of methanol, it is expected that H-bonding can occur with the solvent molecules utilizing both the —OH groups and through the nitrogen atom of the isoxazole ring of the IOC molecule. Upon deuteration, though the H-bonding through the nitrogen atom would be disturbed, that with the —OH group would still remain intact. Since the later one is having the major contribution, the average lifetime in case of methanol-*d*4 was also found to be equivalent to its non-deuterated counterpart.

#### 4. Conclusion

The photophysical properties of isoxazole derivative of curcumin (IOC) have been studied in presence of various polar protic, polar aprotic and non-polar solvents. Herein, the IOC molecule has been proved to bear a planar structure where the electron gets delocalized over the whole molecule. Based on the calculations of the charge distribution it could be confirmed that the nitrogen acquires a partial negative charge whereas oxygen of the isoxazole ring remains partially positively charged. The electronic structure calculations with DFT also demonstrated that the most stable stereoisomer is the one in which both the aliphatic double bonds are having *trans*- geometries; i.e. (*E,E*). Studies of solvatochromism on the IOC molecule revealed that both the absorption and emission maxima experienced a traditional red shift upon increase in the solvent polarity. In case of DMSO, an unexpectedly large red shift in both absorption as well as emission spectra has been analyzed along with the fastest decay of the excited state of the IOC molecule. Based on the RDF analysis on MD trajectories followed by DFT, it has been established that being an H-bond acceptor type of category, DMSO forms a comparatively stronger H-bond with the hydroxyl group of the IOC molecule. Moreover, the slowest fluorescence lifetime of the excited state of IOC has been observed in case of benzene solvent. The MD calculations have also revealed that benzene forms an ordered distribution around the IOC molecule through hydrophobic ( $\pi$ - $\pi$  stacking) interactions. The Fluorescence lifetime studies pointed towards the excited state of IOC molecule relaxing via three probable pathways, with the overall process of decay being comparatively slower in the case of non-polar solvents. Upon deuteration of solvents, no significant changes could be observed in the emission or excitation spectra.

Ultimately, from all these results it could be concluded that H-bonding is not the sole reason for extraordinary photophysics of IOC molecule but rather there is an interplay of factors like solvent polarity, viscosity, dielectric constant, hydrogen bonding ability etc.

### CRedit authorship contribution statement

**Manisha Sharma:** Writing - original draft, Formal analysis, Methodology, Conceptualization, Investigation, Writing - review & editing. **Uttam Pal:** Formal analysis, Methodology, Software, Writing - review & editing. **Mamta Kumari:** Validation, Investigation, Formal analysis, Writing - review & editing. **Damayanti Bagchi:** Validation, Formal analysis. **Swati Rani:** Validation, Formal analysis. **Dipanjan Mukherjee:** Validation, Formal analysis, Writing - review & editing. **Arpan Bera:** Validation, Formal analysis. **Samir Kumar Pal:** Conceptualization, Resources, Validation, Writing - review & editing. **Tanusree Saha Dasgupta:** Conceptualization, Resources, Validation, Software, Writing - review & editing. **Subho Mozumdar:** Conceptualization, Resources, Validation, Writing - review & editing, Supervision.

### Declaration of Competing Interest

The authors declare that they have no known competing financial interests or personal relationships that could have appeared to influence the work reported in this paper.

### Acknowledgements

M.S. acknowledges the UGC, India for the financial support. Thanks are due to the Department of Chemistry, and U.S.I.C., University of Delhi, New Delhi as well as Technical cell, S.N.B.N.C.B.S., Kolkata for providing the instrumentation facility. The authors also thanks DST-SERBEMR/2016/006678, India, for financial support.

### Appendix A. Supplementary data

Supplementary material related to this article can be found, in the online version, at doi:<https://doi.org/10.1016/j.jphotochem.2021.113164>.

### References

[1] A. Marini, A. Muñoz-Losa, A. Biancardi, B. Mennucci, What is solvatochromism? *J. Phys. Chem. B* 114 (51) (2010) 17128–17135.  
 [2] W. Liptay, Electrochromism and solvatochromism, *Angew. Chemie Int. Ed. English* 8 (3) (1969) 177–188.  
 [3] L.C.D. de Rezende, M.M. Vaidergorn, J.C.B. Moraes, F. da Silva Emery, Synthesis, photophysical properties and solvatochromism of meso-substituted tetramethyl BODIPY dyes, *J. Fluoresc.* 24 (1) (2014) 257–266.  
 [4] E. Bozkurt, H.I. Gul, E. Mete, Solvent and substituent effect on the photophysical properties of pyrazoline derivatives: a spectroscopic study, *J. Photochem. Photobiol. A: Chem.* 352 (2018) 35–42.  
 [5] T. Peng, X. Chen, L. Gao, T. Zhang, W. Wang, J. Shen, D. Yang, A rationally designed rhodamine-based fluorescent probe for molecular imaging of peroxynitrite in live cells and tissues, *Chem. Sci.* 7 (8) (2016) 5407–5413.  
 [6] J.L. Westrup, L.W. Oenning, M.M. da Silva Paula, R. da Costa Duarte, F. S. Rodembusch, T.E.A. Frizon, L. da Silva, A.G. Dal-Bó, New photoactive D- $\pi$ -A- $\pi$ -D benzothiadiazole derivative: synthesis, thermal and photophysical properties, *Dye. Pigments* 126 (2016) 209–217.  
 [7] D.-H. Lee, D.-N. Lee, J.-I.A. Hong, Fluorescent probe for a lewisite simulant, *New J. Chem.* 40 (11) (2016) 9021–9024.  
 [8] T. Lopez Arbeloa, F. Lopez Arbeloa, M.J. Tapia, I. Lopez Arbeloa, Hydrogen-bonding effect on the photophysical properties of 7-aminocoumarin derivatives, *J. Phys. Chem.* 97 (18) (1993) 4704–4707.  
 [9] A. Barik, S. Nath, H. Pal, Effect of solvent polarity on the photophysical properties of coumarin-1 dye, *J. Chem. Phys.* 119 (19) (2003) 10202–10208.  
 [10] A.K. Satpati, M. Kumbhakar, D.K. Maity, H. Pal, Photophysical investigations of the solvent polarity effect on the properties of coumarin-6 dye, *Chem. Phys. Lett.* 407 (1–3) (2005) 114–118.  
 [11] S. Nad, H. Pal, Unusual photophysical properties of coumarin-151, *J. Phys. Chem. A* 105 (7) (2001) 1097–1106.

[12] A. Beeby, A.W. Parker, M.S. Simpson, D. Phillips, The effect of solvent deuteration on the photophysics of sulphonated aluminium phthalocyanine, *J. Photochem. Photobiol. B Biol.* 16 (1) (1992) 73–81.  
 [13] S. Paul, P.W.S. Heng, L.W. Chan, Optimization in solvent selection for chlorin e6 in photodynamic therapy, *J. Fluoresc.* 23 (2) (2013) 283–291.  
 [14] P.F. Aramendia, M. Krieg, C. Nitsch, E. Bittersmann, S.E. Braslavsky, The photophysics of merocyanine 540. A comparative study in ethanol and in liposomes, *Photochem. Photobiol.* 48 (2) (1988) 187–194.  
 [15] J. Dey, I.M. Warner, Spectroscopic and photophysical studies of the anticancer drug: camptothecin, *J. Lumin.* 71 (2) (1997) 105–114.  
 [16] D. Karcz, A. Matwijczuk, B. Boron, B. Creaven, L. Fiedor, A. Niewiadomy, M. Gagoś, Isolation and spectroscopic characterization of Zn (II), Cu (II), and Pd (II) complexes of 1, 3, 4-thiadiazole-derived ligand, *J. Mol. Struct.* 1128 (2017) 44–50.  
 [17] I. Budziak, D. Karcz, M. Makowski, K. Rachwał, K. Starzak, A. Matwijczuk, B. Myśliwa-Kurdziel, A. Oniszczuk, M. Combrzyński, A. Podleśna, Non-typical fluorescence effects and biological activity in selected 1, 3, 4-thiadiazole derivatives: spectroscopic and theoretical studies on substituent, molecular aggregation, and pH effects, *Int. J. Mol. Sci.* 20 (21) (2019) 5494.  
 [18] K. Starzak, A. Matwijczuk, B. Creaven, A. Matwijczuk, S. Wybraniec, D. Karcz, Fluorescence quenching-based mechanism for determination of hypochlorite by coumarin-derived sensors, *Int. J. Mol. Sci.* 20 (2) (2019) 281.  
 [19] I. Budziak, D. Karcz, M. Makowski, B. Myśliwa-Kurdziel, K. Kasprzak, A. Matwijczuk, E. Chruściel, A. Oniszczuk, L. Adwent, A. Matwijczuk, Spectroscopic and theoretical investigation into substituent-and aggregation-related dual fluorescence effects in the selected 2-amino-1, 3, 4-thiadiazoles, *J. Mol. Liq.* 291 (2019), 111261.  
 [20] A. Barik, N. Goel, K. Priyadarsini, H. Mohan, Effect of deuterated solvents on the excited state photophysical properties of curcumin, *J. Photosci.* 11 (2004) 95–99.  
 [21] S.M. Khopde, K. Indira Priyadarsini, D.K. Palit\*, T. Mukherjee, Effect of solvent on the excited-state photophysical properties of curcumin, *Photochem. Photobiol.* 72 (5) (2000) 625–631.  
 [22] R. Adhikary, P. Mukherjee, T.W. Kee, J.W. Petrich, Excited-state intramolecular hydrogen atom transfer and solvation dynamics of the medicinal pigment curcumin, *J. Phys. Chem. B* 113 (15) (2009) 5255–5261.  
 [23] A. Goel, A.B. Kunnumakkara, B.B. Aggarwal, Curcumin as “Curcumin”: from kitchen to clinic, *Biochem. Pharmacol.* 75 (4) (2008) 787–809.  
 [24] R.C. Lantz, G. Chen, A. Solyom, S. Jolad, B. Timmermann, The effect of turmeric extracts on inflammatory mediator production, *Phytomedicine* 12 (6–7) (2005) 445–452.  
 [25] A. Abusnina, T. Keravis, I. Yougbaré, C. Bronner, C. Lugnier, Anti-proliferative effect of curcumin on melanoma cells is mediated by PDE1A inhibition that regulates the epigenetic integrator UHRF1, *Mol. Nutr. Food Res.* 55 (11) (2011) 1677–1689.  
 [26] M.E. Egan, M. Pearson, S.A. Weiner, V. Rajendran, D. Rubin, J. Glöckner-Pagel, S. Canny, K. Du, G.L. Lukacs, M.J. Caplan, Curcumin, a major constituent of turmeric, corrects cystic fibrosis defects, *Science* 304 (5670) (2004) 600–602.  
 [27] R.B. Mythri, M.M. Srinivas Bharath, Curcumin: a potential neuroprotective agent in Parkinson's disease, *Curr. Pharm. Des.* 18 (1) (2012) 91–99.  
 [28] S. Mangalathillam, N.S. Rejinold, A. Nair, V.-K. Lakshmanan, S.V. Nair, R. Jayakumar, Curcumin loaded chitin nanogels for skin cancer treatment via the transdermal route, *Nanoscale* 4 (1) (2012) 239–250.  
 [29] F. Payton, P. Sandusky, W.L. Alworth, NMR study of the solution structure of curcumin, *J. Nat. Prod.* 70 (2) (2007) 143–146.  
 [30] C.F. Chignell, P. Bilskj, K.J. Reszka, A.G. Motten, R.H. Sik, T.A. Dahl, Spectral and photochemical properties of curcumin, *Photochem. Photobiol.* 59 (3) (1994) 295–302.  
 [31] C. Ghatak, V.G. Rao, S. Mandal, S. Ghosh, N. Sarkar, An understanding of the modulation of photophysical properties of curcumin inside a micelle formed by an ionic liquid: a new possibility of tunable drug delivery system, *J. Phys. Chem. B* 116 (10) (2012) 3369–3379.  
 [32] C. Hsieh, Phase I clinical trial of curcumin, a chemopreventive agent, in patients with high-risk or pre-malignant lesions, *Anticancer Res.* 21 (2895) (2001) e2900.  
 [33] Y.-J. Wang, M.-H. Pan, A.-L. Cheng, L.-I. Lin, Y.-S. Ho, C.-Y. Hsieh, J.-K. Lin, Stability of curcumin in buffer solutions and characterization of its degradation products, *J. Pharm. Biomed. Anal.* 15 (12) (1997) 1867–1876.  
 [34] P. Anand, A.B. Kunnumakkara, R.A. Newman, B.B. Aggarwal, Bioavailability of curcumin: problems and promises, *Mol. Pharm.* 4 (6) (2007) 807–818.  
 [35] A. Vyas, P. Dandawate, S. Padhye, A. Ahmad, F. Sarkar, Perspectives on new synthetic curcumin analogs and their potential anticancer properties, *Curr. Pharm. Des.* 19 (11) (2013) 2047–2069.  
 [36] A. Jezierska, J. Panek, S. Ryng, DFT study of a novel lead structure in the isoxazole heterocyclic system, *J. Mol. Struct. Theochem.* 636 (1–3) (2003) 203–214.  
 [37] Z. Sui, R. Salto, J. Li, C. Craik, P.R.O. de Montellano, Inhibition of the HIV-1 and HIV-2 proteases by curcumin and curcumin boron complexes, *Bioorg. Med. Chem.* 1 (6) (1993) 415–422.  
 [38] S. Chakraborti, G. Dhar, V. Dwivedi, A. Das, A. Poddar, G. Chakraborti, G. Basu, P. Chakraborti, A. Surolia, B. Bhattacharya, Stable and potent analogues derived from the modification of the dicarbonyl moiety of curcumin, *Biochemistry* 52 (42) (2013) 7449–7460.  
 [39] C. Selvam, S.M. Jachak, R. Thilagavathi, A.K. Chakraborti, Design, synthesis, biological evaluation and molecular docking of curcumin analogues as antioxidant, cyclooxygenase inhibitory and anti-inflammatory agents, *Bioorg. Med. Chem. Lett.* 15 (7) (2005) 1793–1797.  
 [40] M. Labbozzetta, R. Baruchello, P. Marchetti, M.C. Gueli, P. Poma, M. Notarbartolo, D. Simoni, N. D'Alessandro, Lack of nucleophilic addition in the isoxazole and

- pyrazole diketone modified analogs of curcumin; implications for their antitumor and chemosensitizing activities, *Chem. Biol. Interact.* 181 (1) (2009) 29–36.
- [41] P. Poma, M. Notarbartolo, M. Labbozzetta, A. Maurici, V. Carina, A. Alaimo, M. Rizzi, D. Simoni, N. D'Alessandro, The antitumor activities of curcumin and of its isoxazole analogue are not affected by multiple gene expression changes in an MDR model of the MCF-7 breast cancer cell line: analysis of the possible molecular basis, *Int. J. Mol. Med.* 20 (3) (2007) 329–335.
- [42] S. Mishra, K. Karmodiya, N. Suroliya, A. Suroliya, Synthesis and exploration of novel curcumin analogues as anti-malarial agents, *Bioorg. Med. Chem.* 16 (6) (2008) 2894–2902.
- [43] S.A.M. Shaikh, B.G. Singh, A. Barik, N.V. Balaji, G.V. Subbaraju, D.B. Naik, K. I. Priyadarsini, Unravelling the effect of  $\beta$ -diketo group modification on the antioxidant mechanism of curcumin derivatives: a combined experimental and DFT approach, *J. Mol. Struct.* 1193 (2019) 166–176.
- [44] B.K. Sahoo, K.S. Ghosh, S. Dasgupta, Investigating the binding of curcumin derivatives to bovine serum albumin, *Biophys. Chem.* 132 (2–3) (2008) 81–88.
- [45] B.K. Sahoo, K.S. Ghosh, S. Dasgupta, Molecular interactions of isoxazolcurcumin with human serum albumin: spectroscopic and molecular modeling studies, *Biopolym. Original Res. Biomol.* 91 (2) (2009) 108–119.
- [46] S.A.M. Shaikh, B.G. Singh, A. Barik, M.V. Ramani, N.V. Balaji, G.V. Subbaraju, D. B. Naik, K.I. Priyadarsini, Diketo modification of curcumin affects its interaction with human serum albumin, *Spectrochim. Acta A Mol. Biomol. Spectrosc.* 199 (2018) 394–402.
- [47] S. Maity, S. Pal, S. Sardar, N. Sepay, H. Parvej, J. Chakraborty, U.C. Halder, Multispectroscopic analysis and molecular modeling to investigate the binding of beta lactoglobulin with curcumin derivatives, *RSC Adv.* 6 (113) (2016) 112175–112183.
- [48] R. Bera, B.K. Sahoo, K.S. Ghosh, S. Dasgupta, Studies on the interaction of isoxazolcurcumin with calf thymus DNA, *Int. J. Biol. Macromol.* 42 (1) (2008) 14–21.
- [49] M.J. Kamlet, J.L. Abboud, R. Taft, The solvatochromic comparison method. 6. The  $\pi^*$  scale of solvent polarities, *J. Am. Chem. Soc.* 99 (18) (1977) 6027–6038.
- [50] Y. Marcus, The properties of organic liquids that are relevant to their use as solvating solvents, *Chem. Soc. Rev.* 22 (6) (1993) 409–416.
- [51] K.H. Nagachandra, J.R. Mannekutla, S.M. Amarayya, S.R. Inamdar, Solvent effect on the spectral properties of dipolar laser dyes: evaluation of ground and excited state dipole moments, *Eur. J. Chem.* 3 (2) (2012) 163–171.
- [52] G.V. Loukova, V.P. Vasiliev, A.A. Milov, V.A. Smirnov, V.I. Minkin, Unraveling electronic properties of an organometallic solute: Lippert-Mataga and quantum-chemical extensive study, *J. Photochem. Photobiol. A: Chem.* 327 (2016) 6–14.
- [53] G. Dutt, S. Doraiswamy, N. Periasamy, B. Venkataraman, Rotational reorientation dynamics of polar dye molecular probes by picosecond laser spectroscopic technique, *J. Chem. Phys.* 93 (12) (1990) 8498–8513.
- [54] D.R. Lide, *CRC Handbook of Chemistry and Physics: A Ready-reference Book of Chemical and Physical Data*, CRC press, 1995.
- [55] S. Ghosh, J. Kuchlyan, D. Banik, N. Kundu, A. Roy, C. Banerjee, N. Sarkar, Organic additive, 5-methylsalicylic acid induces spontaneous structural transformation of aqueous pluronic triblock copolymer solution: a spectroscopic investigation of interaction of curcumin with pluronic micellar and vesicular aggregates, *J. Phys. Chem. B* 118 (39) (2014) 11437–11448.
- [56] R.F. Kubin, A.N. Fletcher, Fluorescence quantum yields of some rhodamine dyes, *J. Lumin.* 27 (4) (1982) 455–462.
- [57] D. Bagchi, S.K. Pal, Probing crucial interfacial dynamics of nano-hybrids for emerging functionalities. *Nano-hybrids in Environmental & Biomedical Applications*, CRC Press, 2019, pp. 29–58.
- [58] B. Miehlich, A. Savin, H. Stoll, H. Preuss, Results obtained with the correlation energy density functionals of Becke and Lee, Yang and Parr, *Chem. Phys. Lett.* 157 (3) (1989) 200–206.
- [59] Y. Tawada, T. Tsuneda, S. Yanagisawa, T. Yanai, K. Hirao, A long-range-corrected time-dependent density functional theory, *J. Chem. Phys.* 120 (18) (2004) 8425–8433.
- [60] T. Yanai, D.P. Tew, N.C. Handy, A new hybrid exchange–correlation functional using the Coulomb-attenuating method (CAM-B3LYP), *Chem. Phys. Lett.* 393 (1–3) (2004) 51–57.
- [61] B. Mennucci, J. Tomasi, R. Cammi, J. Cheeseman, M. Frisch, F. Devlin, S. Gabriel, P. Stephens, Polarizable continuum model (PCM) calculations of solvent effects on optical rotations of chiral molecules, *J. Phys. Chem. A* 106 (25) (2002) 6102–6113.
- [62] P. Homem-de-Mello, B. Mennucci, J. Tomasi, A. Da Silva, The effects of solvation in the theoretical spectra of cationic dyes, *Theor. Chem. Acc.* 113 (5) (2005) 274–280.
- [63] R. Jin, W. Sun, S. Tang, A DFT study of pyrrole-isoxazole derivatives as chemosensors for fluoride anion, *Int. J. Mol. Sci.* 13 (9) (2012) 10986–10999.
- [64] K.J. Bowers, D.E. Chow, H. Xu, R.O. Dror, M.P. Eastwood, B.A. Gregersen, J. L. Klepeis, I. Kolossvary, M.A. Moraes, F.D. Sacerdoti, In calable algorithms for molecular dynamics simulations on commodity clusters, in: *SC'06: Proceedings of the 2006 ACM/IEEE Conference on Supercomputing*, IEEE, 2006 pp 43–43.
- [65] E. Harder, W. Damm, J. Maple, C. Wu, M. Reboul, J.Y. Xiang, L. Wang, D. Lupyan, M.K. Dahlgren, J.L. Knight, OPLS3: a force field providing broad coverage of drug-like small molecules and proteins, *J. Chem. Theory Comput.* 12 (1) (2015) 281–296.
- [66] U. Pal, S.K. Pramanik, B. Bhattacharya, B. Banerji, N.C. Maiti, Binding interaction of a gamma-aminobutyric acid derivative with serum albumin: an insight by fluorescence and molecular modeling analysis, *SpringerPlus* 5 (1) (2016) 1121.
- [67] S. Rani, D. Bagchi, U. Pal, M. Kumari, M. Sharma, A. Bera, J. Shabir, S.K. Pal, T. Saha-Dasgupta, S. Mozumdar, The role of imidazolium-based surface-active ionic liquid to restrain the excited-state intramolecular H-Atom transfer dynamics of medicinal pigment curcumin: a theoretical and experimental approach, *ACS Omega* 5 (40) (2020) 25582–25592.
- [68] B. Varghese, S.N. Al-Busafi, F.O. Suliman, S.M. Al-Kindy, Study on the spectral and inclusion properties of a sensitive dye, 3-naphthyl-1-phenyl-5-(5-fluoro-2-nitrophenyl)-2-pyrazoline, in solvents and  $\beta$ -cyclodextrin, *Spectrochim. Acta A. Mol. Biomol. Spectrosc.* 136 (2015) 661–671.
- [69] N. Patil, R.M. Melavanki, S. Kapatkar, N. Ayachit, J. Saravanan, Solvent effect on absorption and fluorescence spectra of three biologically active carboxamides (C 1, C 2 and C 3). Estimation of ground and excited state dipole moment from solvatochromic method using solvent polarity parameters, *J. Fluoresc.* 21 (3) (2011) 1213–1222.
- [70] K.I. Priyadarsini, Photophysics, photochemistry and photobiology of curcumin: studies from organic solutions, bio-mimetics and living cells, *J. Photochem. Photobiol. C Photochem. Rev.* 10 (2) (2009) 81–95.
- [71] O.S. Hammond, D.T. Bowron, K.J. Edler, Liquid structure of the choline chloride-urea deep eutectic solvent (reline) from neutron diffraction and atomistic modelling, *Green Chem.* 18 (9) (2016) 2736–2744.
- [72] M. Saha, M.S. Rahman, M.N. Hossain, D.E. Rainie, M.A. Halim, Molecular and spectroscopic insights of a choline chloride based therapeutic deep eutectic solvent, *J. Phys. Chem. A* 124 (23) (2020) 4690–4699.
- [73] R. Yip, Y. Wen, A. Szabo, Decay associated fluorescence spectra of coumarin 1 and coumarin 102: evidence for a two-state solvation kinetics in organic solvents, *J. Phys. Chem.* 97 (40) (1993) 10458–10462.
- [74] H.N. Ghosh, Charge transfer emission in coumarin 343 sensitized TiO<sub>2</sub> nanoparticle: a direct measurement of back electron transfer, *J. Phys. Chem. B* 103 (47) (1999) 10382–10387.
- [75] G. Jones, W.R. Jackson, C.Y. Choi, W.R. Bergmark, Solvent effects on emission yield and lifetime for coumarin laser dyes. Requirements for a rotatory decay mechanism, *J. Phys. Chem.* 89 (2) (1985) 294–300.
- [76] S. Nad, M. Kumbhakar, H. Pal, Photophysical properties of coumarin-152 and coumarin-481 dyes: unusual behavior in nonpolar and in higher polarity solvents, *J. Phys. Chem. A* 107 (24) (2003) 4808–4816.